

Title	Highly soluble and well-defined polysaccharide- based micelle in aqueous media: Decyl succinic anhydride-modified pullulan
Author(s)	Suenaga, Risa; Komuro, Yuzu; Terao, Ken
Citation	Carbohydrate Polymers. 2025, 358, p. 123504
Version Type	VoR
URL	https://hdl.handle.net/11094/100612
rights	This article is licensed under a Creative Commons Attribution 4.0 International License.
Note	

The University of Osaka Institutional Knowledge Archive : OUKA

https://ir.library.osaka-u.ac.jp/

The University of Osaka

ELSEVIER

Contents lists available at ScienceDirect

Carbohydrate Polymers

journal homepage: www.elsevier.com/locate/carbpol





Highly soluble and well-defined polysaccharide-based micelle in aqueous media: Decyl succinic anhydride-modified pullulan

Risa Suenaga, Yuzu Komuro, Ken Terao

Department of Macromolecular Science, Graduate School of Science, Osaka University, 1-1 Machikaneyama-cho, Toyonaka, Osaka 560-0043, Japan

ARTICLE INFO

Keywords: Amphiphilic polysaccharide derivative Pullulan Flower micelle Small-angle X-ray scattering Light scattering

ABSTRACT

A pullulan-based polymeric micelle was obtained by modifying pullulan with decyl succinic anhydride (PulDS) to achieve a degree of substitution ranging from 0.46 to 0.72. SEC-MALS, static and dynamic light scattering, small angle X-ray scattering (SAXS), and fluorescence measurements were performed to characterize the micelle structure of PulDS in 25 mM aqueous NaCl at two different pH of 7 and 10. The scattering and fluorescence data clearly showed that the PulDS is molecularly dispersed as flower necklace micelles in the aqueous solvents. The size distribution of the unit micelles is significantly narrower than that of the previously investigated succinic anhydride modified pullulan. The resulting unit micelle size was found to depend less on chain length and degree of substitution, but the unit flower micelle was larger at pH 7 than at pH 10, suggesting that excess ionized OH groups on the glycosidic ring provide repulsive forces between the polymer chains. These features, namely the well-defined micelle structure and high solubility in aqueous media without large aggregates, indicate potential applications in drug delivery systems and as food additives.

1. Introduction

Since large amounts of different polysaccharides are available from natural organisms, the chemical modification of polysaccharides is one of the most important industrial and research areas of polymeric materials. Among them, hydrophobically modified polysaccharides are intensively developed because of their use as food additives and drug carriers due to their controlled nanostructures in aqueous media (Wu et al., 2022). While block copolymer systems consisting of hydrophobic and hydrophilic chains tend to form well-defined core-shell micelles, polysaccharides grafted with hydrophobic groups exhibit a greater variety of structures.

Hydrophobic succinate polysaccharides are a class of polysaccharide derivatives. They contain both an ionic group and a hydrophobic chain on each substituted group. Octenylsuccinated derivatives of starch (Sweedman et al., 2013), hyaluronic acid (Eenschooten et al., 2012; Mayol et al., 2014), oat β -glucan (Wu et al., 2019; Wu et al., 2020), hydroxypropyl acidolysis tamarind gum (Hongbo et al., 2022), and dextran (Ridella et al., 2024) have been extensively studied to confirm their micellar structures as well as their versatile applications, including use as food additives and drug delivery systems. However, structural characterization using light and X-ray scattering has not yet been

established, although the micelle structure of vinyl-polymer-based amphiphilic polymers is well described in terms of the flower micelle and/or flower necklace model (Uramoto et al., 2016). Recently, the polymer micelles have garnered interest for biomedical applications, including the use as drug (Cao et al., 2023; Liang et al., 2024) and gene carriers (Zhou et al., 2024). Structural characterization in aqueous media will play an important role in the development of polysaccharide-based polymer micelles in order to accurately and efficiently deliver the target compounds to the site of interest.

Recently, Yang et al. investigated the micellar structure of octenyl (Yang & Sato, 2020b, 2021a, 2021b), nonenyl (Yang et al., 2024), and decenyl (Li et al., 2025) succinic anhydride-modified pullulans, where pullulan, an exopolysaccharide with high water solubility, has seen a rapid increase in production and various applications in recent years (Aquinas et al., 2024; Cruz-Santos et al., 2023; de Souza et al., 2023; Ganie et al., 2024; Prajapati et al., 2013; Sonam Jain et al., 2013; Thakur et al., 2023). The dimensional properties estimated from scattering measurements, together with the fluorescence behavior of pyrene, can be explained by the flower necklace model (Sato et al., 2022). However, the size distribution of the micelles is significantly broader than that of the previously studied vinyl polymers (Kono et al., 2023; Uramoto et al., 2016) and, in addition, a not insignificant amount of large aggregates

E-mail address: terao.ken.sci@osaka-u.ac.jp (K. Terao).

^{*} Corresponding author.

affected the scattering data. Such aggregates may obscure the accurate determination of the micelle structure. It is also suggested that the broad distribution of the micelle structure makes it difficult to characterize the micelles structurally, considering that non-spherical assemblies have been proposed for some amphiphilic polysaccharide derivatives (Ikkene et al., 2020; Kameyama et al., 2019; Nishimura et al., 2020; Nishimura et al., 2021; Six & Ferji, 2019). Consequently, it is desirable to obtain uniformly sized micelles with few large aggregates to accurately determine their solution structures. In addition, large aggregates might interfere with the accurate delivery of the target compound when applied as drug and/or gene carriers. Furthermore, chemical instability of unsaturated alkyl side groups may affect the aggregating behavior.

In this study, we prepared decyl succinic anhydride-modified pullulan (PulDS), whose chemical structure is shown in Fig. 1. To the best of our knowledge, this is the first study on the micelle structure of polysaccharides modified with saturated succinic anhydride. It was initially unexpected that the resulting PulDS samples, with an appropriate degree of substitution, exhibited high solubility in aqueous media without aggregation and a significantly narrower dispersed micelle structure. Consequently, we determined their dimensional and hydrodynamic properties, as well as their complex formation behavior with pyrene, in order to characterize the micellar structure and the hydrophobic portion within the polymer assemblies under two different pH conditions at 25 °C.

2. Experimental section

2.1. Samples

A pullulan sample was purchased from TCI. The sample was fractionally precipitated using water as the solvent and methanol as the precipitant, resulting in two pullulan samples. The concentrated pullulan solution was dialyzed using a Spectrum SPECTRA/POR regenerated cellulose dialysis tube (MWCO = 12,000–14,000) to remove low-molar-mass impurities, including methanol. The solution was then lyophilized to obtain a white solid sample. The two resulting pullulan samples, P266K and P461K, were characterized by size exclusion chromatography (Shodex GPC-101) equipped with a Wyatt DAWN HELEOS II multi-angle light scattering photometer (SEC-MALS), for which the wavelength λ_0 in a vacuum of the incident light was 658 nm, and a Shodex refractive index detector. The eluent used was 50 mM aqueous NaNO3 at a flow rate of 1.0 mL/min. Three columns were connected in series: one guard column (SE-6B) and two analytical columns (OHpak SB-806 HQ, Shodex). The temperature of the column oven

was 40 °C. The refractive index increment $(\partial n/\partial c)$ of the sample at $\lambda_0=658$ nm was estimated to be 0.150 mL/g in the solvent at 25 °C, using a Schulz-Cantow type differential refractometer in the concentration range between 0 and 10 mg/mL.

Six PulDS samples were prepared from the two pullulan samples, P266K and P461K, in an organic solvent system. A detailed procedure for one PulDS sample, P266DS60, is as follows. 2.0 g of P266K sample (12 mmol in glucose unit) and 2.0 g of LiCl (Fujifilm-Wako Co.) were added to a two-necked flask and dried under vacuum at 90 $^{\circ}$ C for 3 h. 80 mL of N,N,-dimethylacetamide (DMF, dehydrated grade, Fujifilm) was added under an Ar atmosphere to dissolve pullulan in the DMF-LiCl solvent. Pyridine (80 mL) and decylsuccinic anhydride (DSA, 3.55 g, 14.8 mmol) were added to the flask. We chose this solvent system instead of aqueous solvent because of the high melting point of DSA. In this regard, similar solvent systems were applied to synthesize various fully substituted (Kishimoto et al., 2022; Kubota et al., 2000) and partly substituted (Kimura et al., 2020; Kobayashi & Terao, 2024; Nakata et al., 2024) polysaccharide carbamate derivatives. The mixture was stirred at 90 °C for 24 h. The obtained brown colored solution was poured into 2 L of diethyl ether to reprecipitate the PulDS sample. The solid sample was dried in a vacuum overnight and purified by reprecipitation with methanol as solvent and water as precipitant. The dried solid sample was dissolved in 50 mM aqueous NaOH. A small amount of the insoluble portion was removed by filtration. The aqueous solution was dialyzed against pure water for at least 4 d to remove soluble low-molar-mass impurities. The aqueous solution of P266DS60 was condensed by a rotary evaporator and lyophilized to obtain a white solid sample. The other PulDS samples were prepared by the same procedure with different molar ratios of DSA to glucose unit, i.e. 1.18, 1.08, 0.50, 1.01, 0.80, and, 0.61 for P266DS60, P266DS24, P266DS14, P461DS72, P461DS46, and P461DS30, respectively, with the amount of polysaccharide sample fixed in each synthesis. It is noted that the methanolwater reprecipitation process was omitted due to their high solubility of the unpurified samples in water.

 ^1H NMR measurements were made on a JEOL ECS400 spectrometer (400 MHz) for 10 mg/mL solution of PulDS in D₂O at 80 °C. The ^1H NMR spectrum for **P266DS60** is shown in Fig. S1 in the Supporting Information. The degree of substitution was estimated from the area ratio of peak (a, assigned to the three protons on the terminal methyl group) to peaks (b, assigned to the six protons on the glycosidic ring excluding the H-1 proton) as described in the previous research (Yang & Sato, 2020b). However, the b peaks for the high DS samples are significantly broader than those for the low DS samples, as shown in Fig. S2. Although the molar mass of a starch derivative was significantly reduced, deuterated

Fig. 1. Chemical structure of PulDS.

dimethylsulfoxide (d_6 -DMSO) with a small amount of deuterated trifluoroacetic acid (d_1 -TFA) can be used as a solvent to determine the DS (Tizzotti et al., 2011). We thus carried out 1 H NMR measurements on **P266DS60**, **P461DS72**, and **P461DS46** in d_6 -DMSO containing 10 wt% d_1 -TFA at 80 °C. The resulting data are shown in Fig. S3 in the Supporting Information, where the peak corresponding to the six protons in the glycosidic ring, appearing between 3.0 and 3.9 ppm (Bruneel et al., 1993) is considerably clearer than that in D₂O. The evaluated DS value and sample yield are summarized in Table 1. The resulting DS values are 12–18 % lower than those in D₂O. This is most likely due to the underestimation of the six protons on the glycosidic ring in D₂O.

The table also contains the solubility in water; all samples were water-soluble, while slight turbidity was observed for P266DS24 and P266DS14. Interestingly, while the original pullulan and high-DS samples were soluble in both water and 50 mM aqueous NaCl, the low DS samples, P266DS24, P266DS14, and P461DS30 were insoluble in 50 mM aqueous NaCl.

SEC-MALS measurements were also performed on the three high DS PulDS samples, **P266DS60**, **P461DS72**, and **P461DS46**, using the same equipment described above for the determination of $M_{\rm w}$ and D. The eluents were 25 mM and 50 mM aqueous NaCl, the flow rate was set at 1.0 mL/min, and the temperature of the column oven was controlled at 40 °C. The excess refractive indices were also measured with the refractometer described above to determine $\partial n/\partial c$ for the three samples in the two solvents at different λ_0 . The values are between 0.144 mL/g and 0.147 mL/g in 25 mM and 0.142 mL/g, and 0.148 mL/g in 50 mM aqueous NaCl, depending slightly on the sample. It is noted that we chose non-dialyzed solution to estimate $\partial n/\partial c$ because the eluent of light scattering measurement of SEC-MALS should be close to the dialyzed solution.

For the following measurements in aqueous NaCl, test solutions were prepared as previously described (Kameyama et al., 2019). Specifically, a PulDS sample was dissolved in pure water at 80 °C for 30 min and stirred overnight at room temperature. The resulting solution was mixed with the same volume of 50 mM aqueous NaCl. The resulting solution was diluted with 25 mM aqueous NaCl to prepare test solutions with different polymer mass concentrations c. We also prepared PulDS solution in aqueous NaCl-NaOH solution at pH = 10 and at [Na $^+$] = 25 mM by adding a small amount of 25 mM aqueous NaOH to the 25 mM aqueous NaCl solution of PulDS. The pH of the resulting solution was confirmed using a Horiba F-54 pH meter. Notably, the pH of PulDS in 25 mM aqueous NaCl was substantially 7 during the measurements described below.

Molecular characteristics of pullulan and PulDS samples.

Sample	Yield /%	Solubility ^a	DS^{b}	$M_{\rm w}$ / kg $ m mol^{-1}$	D	$n_{ m w}^{ m g}$	$A_{2,\mathrm{app}}^{\mathrm{h}}$	$A_{2,\mathrm{app}}^{\mathrm{i}}$
P266K	_	S	_	266 ^e	1.14 ^e	1640	_	-
P461K	_	S	_	461 ^e	1.21 ^e	2850	_	_
P266DS60	54	S	0.68 ^c 0.60 ^d	300^{f}	$1.3^{\rm f}$	939	0.83	2.81
P266DS24	37	I	0.24 ^c	_	_	_	_	_
P266DS14	34	I	0.14 ^c	_	_	_	_	_
P461DS72	63	S	0.86^{c} 0.72^{d}	641 ^f	1.4 ^f	1830	1.13	1.64
P461DS46	58	S	0.56 ^c 0.46 ^d	449 ^f	1.3 ^f	1590	1.15	2.07
P461DS30	56	S	0.30°	_	_	_	_	_

 $^{^{\}rm a}$ In 50 mM aqueous NaCl, c=10 mg/mL. S: soluble. I: insoluble.

2.2. Static and dynamic light scattering (SLS and DLS)

SLS and DLS measurements were carried out for the three high DS PulDS samples, P266DS60, P461DS72, and P461DS46, and one low DS sample, P461DS30, in 25 mM aqueous NaCl and in aqueous NaCl-NaOH solution ([Na $^+$] = 25 mM) at pH = 10, both at 25 °C using an ALV/SLS/ DLS-5000 light scattering photometer (ALV) and vertically polarized incident light from a Nd:YAG laser (250 mW) at $\lambda_0 = 532$ nm. The excess scattering intensities R_{θ} at the scattering angle θ were determined from SLS measurements as a function of c and the magnitude q of the scattering vector, which can be calculated from θ , λ_0 , and the refractive index of the solvent. The intensity autocorrelation function obtained from the DLS measurements was analyzed using the CONTIN method to evaluate the spectrum $A(R_{H,app})$ as a function of the apparent hydrodynamic radius $R_{\rm H,app}$, which can be calculated using the Stokes-Einstein equation. The $\partial n/\partial c$ values at $\lambda_0 = 532$ nm were essentially the same as those at 658 nm described above. The effect of preferential adsorption effect is described below. We also attempted to measure SLS and DLS for PulDS samples in methanol and N,N-dimethylformamide to estimate the molar mass, although we did not analyze the data due to high scattering intensity from large aggregates, suggesting that these solvents are not suitable for the characterization of PulDS.

2.3. Small-angle X-ray scattering (SAXS)

SAXS measurements were performed on PulDS samples in 25 mM aqueous NaCl and in aqueous NaCl-NaOH (pH 10, [Na⁺] = 25 mM) both at 25 °C at the BL40B2 beamline in SPring-8 (Hyogo, Japan). The intensity of the incident X-ray at $\lambda_0 = 0.1$ nm was detected both upstream and downstream of the solution cell to compensate for the intensity fluctuation and transmission of the X-ray. The polymer solutions with four different c and the corresponding solvent were filled into a specially designed quartz capillary cell with a pass length of 2 mm for the SAXS measurements in order to properly subtract the scattered intensity of the solvent from that of the solution. The scattered X-rays were detected using a Dectris Pilatus 3 2 M photon counter located 4.2 m downstream of the solution cell. The diffraction pattern of silver behenate placed at the sample position was used to determine the q value of each pixel on the detector. SAngler software (Shimizu et al., 2016) was utilized to calculate the scattering intensity as a function of the magnitude *q* of the scattering vector. For a wide-angle detector, a solution was also used to evaluate the scattering intensity data over a wider q range. The ratio R_q K' of the reduced scattering intensity R_a to the optical constant K' of X-

^b DS = 3 for full substitution.

 $^{^{\}rm c}\,$ Estimated from $^1{\rm H}$ NMR in ${\rm D_2O.}$

 $^{^{}m d}$ Estimated from $^{
m 1}$ H NMR in $d_{
m 6}$ -DMSO with 10 wt% $d_{
m 1}$ -TFA.

e From SEC-MALS in 50 mM aqueous NaNO₃.

 $^{^{\}rm f}$ Average values from SEC-MALS in 25 mM and 50 mM aqueous NaCl.

 $^{^{\}rm g}$ Calculated from $M_{\rm w}$ and DS.

 $^{^{\}rm h}\,$ From SLS in 25 mM aqueous NaCl. In unit of $10^{-4}\, mol\ m^3\ kg^{-2}.$

ⁱ From SLS in pH 10 aqueous solution with $[Na^+] = 25$ mM. In unit of 10^{-4} mol m³ kg⁻².

rays was estimated from the known relationship (Glatter & Kratky, 1982), using a TOSOH polyethylene oxide standard SE-5, as recently reported (Nakata et al., 2024). To estimate the SAXS contrast factor Δz , the solution density was measured using an Anton Paar DMA-5000 density meter with c range from 0 to 10 mg/mL to estimate the partial specific volume in each solvent.

2.4. Fluorescence of pyrene as a probe of hydrophobicity

To estimate the hydrophobic environment in solution, steady-state fluorescence and fluorescence decay measurements for the pyreneprobed PulDS samples were performed on a HORIBA FluoeoMax-4 fluorescence spectrometer and a HORIBA DeltaPro lifetime spectrofluorometer, respectively, with a 10 mm rectangular quartz cell. A few drops of saturated pyrene-methanol solution was added to the PulDS in 25 mM aqueous NaCl and stirred overnight before fluorescence measurement. The absorbance of the solution at $\lambda_0 = 337$ nm was also measured using a JASCO V-550 UV/vis spectrometer to determine the molar concentration of pyrene [Py]. Three different [Py] were chosen for each PulDS sample. For the fluorescence decay measurement, the incident light at $\lambda_0 = 337$ nm was used and the fluorescence from pyrene molecules at approximately $\lambda_0 = 400$ nm was monitored using a bandpass filter and a cut-off filter placed between the detector and the solution cell to determine the fluorescence intensity I(t) as a function of the decay time t.

3. Results and discussion

3.1. Molar mass and solubility of PulDS in aqueous NaCl

Fig. 2 illustrates the SEC-chromatogram for the three samples in 25 mM aqueous NaCl. A single peak was observed for the three samples. The weight-average molar mass $M_{\rm w}$ and the dispersity index D, defined

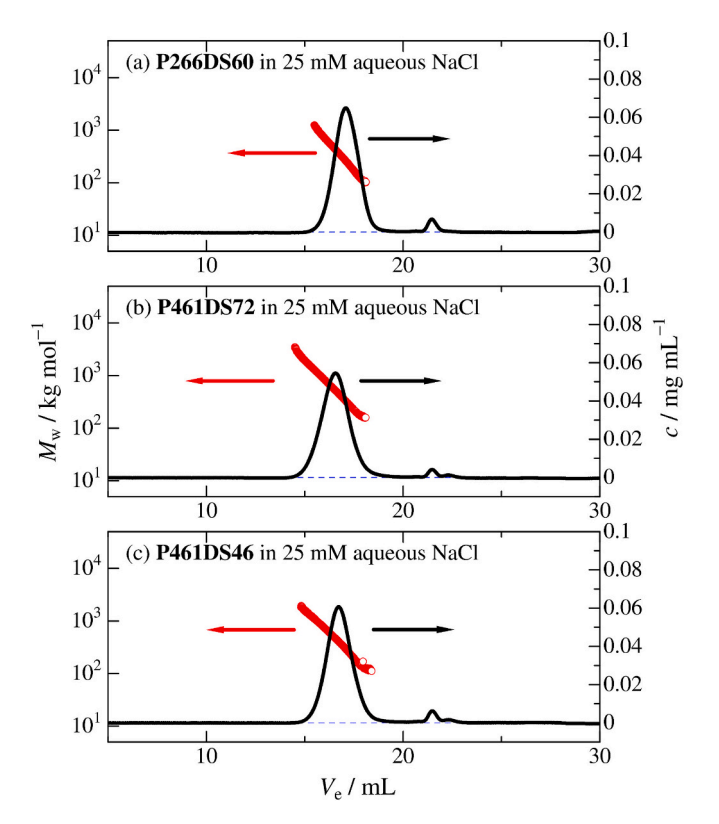


Fig. 2. SEC chromatogram and weight average molar mass $M_{\rm w}$ plotted against elution volume $V_{\rm e}$ for (a) P266DS60, (b) P461DS72, and (c) P461DS46 in 25 mM aqueous NaCl.

as the ratio of $M_{\rm w}$ to the number-average molar mass $M_{\rm p}$, were calculated from the chromatogram where the molar mass at each elution volume was estimated from the scattering intensity of the MALS detector. Substantially the same chromatogram was also obtained in 50 mM aqueous NaCl and different polymer mass concentrations, as shown in Figs. S4 and S5 in the supporting information. Since the evaluated $M_{\rm W}$ and D are essentially the same at different c and solvents, the average $M_{\rm w}$ and D values are summarized in Table 1. This result also clearly indicates that the PulDS samples are molecularly dispersed in the aqueous NaCl solvents, as the $M_{\rm w}$ value in the two solvents may differ when PulDS forms aggregates in the aqueous NaCl solution. The degree of polymerization n_w calculated from the M_w and DS values is somewhat lower than that of the original pullulan samples, suggesting a slight scission of the main chain during sample preparation and/or preferential recovery of lower molar mass components during the synthesis and purification process.

The high solubility in aqueous NaCl was also confirmed by SLS and DLS data. Fig. 3 shows the scattering intensity distribution of the apparent hydrodynamic radius $R_{\rm H,app}$. A single peak in each spectrum is found for the high DS samples, P266DS60, P461DS72, and P461DS46. Similar results were found for the samples in the other solvent at pH = 10. The hydrodynamic radius $R_{\rm H}$ for each sample and solvent was then estimated from the double extrapolation to q = 0 and c = 0 as illustrated in Fig. S6 and the values are summarized in Tables 2 and 3 for those in 25 mM aqueous NaCl and in aqueous NaCl-NaOH solution (pH 10, [Na⁺] = 25 mM), respectively. The unimodal peak for the samples is consistent with molecularly dispersed PulDS in aqueous media while that for P461DS30 is bimodal, suggesting a small amount of large aggregates. Considering that the other two low DS PulDS samples, P266DS24 and P266DS14, were poorly soluble in aqueous NaCl, only PulDS with a certain range of DS can be molecularly dispersed in aqueous NaCl.

The scattering intensity data R_θ/Kc , where K is the optical constant, were also analyzed in terms of Guinier plots as shown in Fig. S7. While the radius of gyration is too small to be determined from the SLS data, the apparent weight-average molar mass $M_{\rm w,app}$ and the apparent second virial coefficient $A_{\rm 2,app}$ were determined. The evaluated $M_{\rm w,app}$ values were systematically between 20 and 30 % lower than the $M_{\rm w}$ value in Table 1, suggesting that preferential adsorption is not negligible, but the molecular dispersion of PulDS can be confirmed. In this study, we do not quantitatively consider this effect in our experiments with the dialyzed PulDS solutions, since even a slight difference in the solvent may influence the micellar structure, as discussed later. $A_{\rm 2,app}$ values are also summarized in Table 1. Regardless of the sample, $A_{\rm 2,app}$ at pH = 10 is about twice as high as that in aqueous NaCl, suggesting a different solvent quality of the two solvents for PulDS.

SAXS scattering intensities for PulDS samples in 25 mM aqueous NaCl are shown in Fig. 4(a), where the excess scattering intensity $\Delta I(q)$ is plotted against q in a double logarithmic fashion. Sharp minima are found for the three high DS samples, P461DS72 P266DS60, and P461DS46, while only a very weak minimum is found for the other three samples. The former sharp minimum is comparable to the SAXS data for core-shell micelles formed by block copolymers (Narita et al., 2004) and alternative and/or random copolymers (Kono et al., 2023; Uramoto et al., 2016), indicating micelle formation. Interestingly, it is much deeper than the previously investigated pullulan derivatives with unsaturated alkyl groups (Li et al., 2025; Yang et al., 2024; Yang & Sato, 2020b) in aqueous media. In this regard, no significant minima were found for the cholesterol-bearing pullulan with low DS developed by Akiyoshi et al. (Akiyoshi et al., 1993), while only a compact conformation of these nanogels in aqueous solution was revealed by dynamic light scattering and neutron scattering (Inomoto et al., 2009). Furthermore, the essentially flat region in the low q end for the high DS samples is consistent with small $R_{\rm g}$ as described for the SLS data mentioned above. On the contrary, for the low DS samples, significant increases in $\Delta I(q)$ with decreasing q clearly indicate the presence of the large

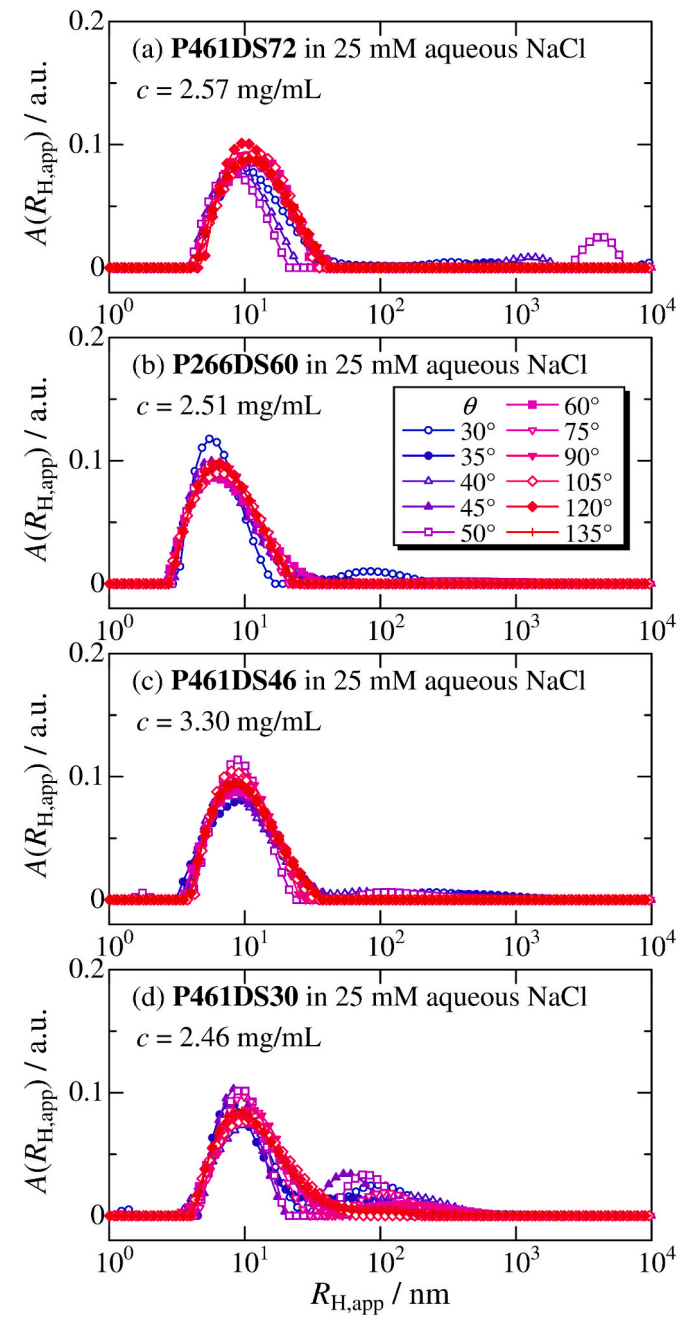


Fig. 3. DLS results for (a) P461DS72, (b) P266DS68, (c) P461DS46, and (d) P461DS30 in 25 mM aqueous NaCl at indicated scattering angles at 25 $^{\circ}$ C.

aggregates. This is in agreement with the DLS data mentioned above. On the other hand, the SAXS data in the other solvent at pH 10 shown in Fig. 4(b) have a similar tendency, while the q value at the minimum ΔI

(q) is systematically larger for the high-DS samples than for those at neutral pH, suggesting that PulDS with high DS tends to have a micellar structure, which can be affected by pH.

As shown in Fig. S8 no substantial concentration dependence was found for $\Delta I(q)$ data for the three high DS PulDS samples in the two solvents except for the low q end, indicating that the local micelle structure is not affected by c in the investigated c range of 2 to 10 mg/ mL, because the slight c dependence of $\Delta I(q)$ can be classified as the influence of A_2 . Thus, we extrapolated to infinite dilution and the converted absolute scattering intensity $R_q/K'c$ is analyzed by the Guinier plot as shown in Fig. S9 the evaluated R_g data from the initial slope are listed in Tables 2 and 3. The apparent weight-average molar mass $M_{w,app}$ estimated from the intercept is systematically smaller than $M_{\rm w}$ in Table 1, while they are only 2-3 % smaller than those determined from SLS. This suggests that the evaluated scattering data reflect molecularly dispersed PulDS micelles for all three high DS samples in the two solvents. Considering that large polydisperse aggregates was observed for the previously investigated pullulan derivatives with unsaturated alkyl groups (Li et al., 2025; Yang et al., 2024; Yang & Sato, 2020b), PulDS may serve as a good model polysaccharide derivative for investigating polysaccharide-based micelles.

3.2. Hydrophobicity of PulDS in aqueous NaCl deduced from fluorescence of pyrene

Pyrene in aqueous PulDS solution tends to accumulate in the hydrophobic part or micelle core of PulDS and the fluorescence spectra reflects hydrophobicity around the pyrene molecules. The peak ratio I_3 / I_1 of the third ($\lambda_0 = 383$ nm) to the first ($\lambda_0 = 372$ nm) vibronic peaks is used as an indicator of the presence of micelle cores (Goddard et al., 1985) because the value reported for an aqueous micelle solution of sodium dodecyl sulfate is 0.96 (Lianos & Zana, 1980), which is much higher than 0.6 in bulk water (Kalyanasundaram & Thomas, 1977). The fluorescence spectra of pyrene in the presence of PulDS are shown in Fig. 5. Similar spectra were observed in the ultraviolet region, and a broad peak of pyrene excimer is found in the visible light region. This is also a typical spectral feature of polymer micelles. The obtained ratio I_3 / I₁ values were almost independent of [Py], indicating good repeatability. The evaluated I_3/I_1 are plotted against DS in Fig. 5(e) where DS_{hydrophobic} denotes the degree of substitution of the hydrophobic group, and has the same meaning as DS for PulDS. The much higher I_3/I_1 values than that in water and hydrophilic sodium carboxymethyl amylose (0.68, (Kameyama et al., 2019)) indicate the presence of micelle core for PulDS in aqueous NaCl. The almost no DS dependence of the I_3/I_1 data for the current PulDS indicates the existence of a stable micelle core in the DS region. The resulting I_3/I_1 is essentially the same as that of octenyl succinic anhydride-modified pullulan (PULOSA) (Yang & Sato, 2020b, 2021b), while it is smaller than that of amylose bearing dodecyl ether and sodium carboxymethyl groups (C12CMA) (Kameyama et al., 2019). This difference may be because both hydrophobic and ionic groups are substituted on the same OH group of pullulans for PulDS and PULOSA, while the hydrophobic site for C12CMA is located at different sites on the carboxymethyl groups (Kameyama et al., 2019).

Table 2 Micelle parameters PulDS samples in 25 mM aqueous NaCl at 25 $^{\circ}$ C.

Sample	$R_{\rm H}/{\rm nm}^{\rm a}$	$R_{\rm g}/{\rm nm}^{\rm b}$	$\Delta ho_{ m r}^{ m c}$	$R_{\rm C,m}/{\rm nm}^{\rm c}$	$R_{\rm O,m}/{\rm nm}^{\rm d}$	σ^{c}	$n_{\rm c}{}^{\rm c}$	$L_{\rm K,FN}$ / nm $^{\rm c}$	$I_3/I_1^{\mathbf{d}}$	$n_{ m hp}^{ m d}$
P461DS72	12.2	9.8	-3.7 ± 1.0	1.13 ± 0.09	2.25 ± 0.15	0.14 ± 0.05	10.5 ± 1.0	30 ± 10	0.93	22 ± 2
P266DS60 P461DS46	6.5 10.2	7.5 9.6	-2.9 ± 0.7 -3.4 ± 0.9	1.37 ± 0.12 1.15 ± 0.10	2.49 ± 0.13 2.27 ± 0.13	0.16 ± 0.05 0.16 ± 0.05	6.0 ± 0.5 10.0 ± 0.5	$\begin{array}{c} 15\pm 5 \\ 30\pm 10 \end{array}$	0.92 0.91	21 ± 3 20 ± 5
1 4010540	10.2	5.0	−3.4 ± 0.5	1.13 ± 0.10	2.27 ± 0.13	0.10 ± 0.05	10.0 ± 0.5	30 ± 10	0.71	20 ± 3

^a From DLS data.

^b From Guinier plot of SAXS data.

 $^{^{}m c}$ Estimated from SAXS profile assuming $\emph{d}_{
m S}=1.12\pm0.2$ nm.

^d Calculated from $R_{O,m} = R_{C,m} + d_S$ considering the error range of d_S .

Table 3 Micelle parameters PulDS samples in aqueous NaCl-NaOH solution (pH 10, $[\mathrm{Na^+}] = 25 \mathrm{\ mM}$).

Sample	R _H /nm ^a	$R_{\rm g}$ /nm ^b	$\Delta ho_{ m r}^{ m \ b}$	$R_{\rm C,m}/{\rm nm}^{\rm b}$	$R_{O,m}/nm^b$	$\sigma^{ m b}$	$n_{\rm c}^{\ c}$	$L_{\rm K,FN}$ / nm ^b
P461DS72 P266DS60	15.4 9.6	$\begin{array}{c} 11\pm1 \\ 8.7 \end{array}$	$-4.1 \pm 1.2 \\ -3.9 \pm 1.1$	$\begin{array}{c} 0.94 \pm 0.10 \\ 0.97 \pm 0.10 \end{array}$	$\begin{array}{c} 2.06 \pm 0.13 \\ 2.09 \pm 0.13 \end{array}$	$\begin{array}{c} 0.14 \pm 0.05 \\ 0.16 \pm 0.05 \end{array}$	$\begin{array}{c} 13\pm1 \\ 8.0\pm0.7 \end{array}$	$30\pm10\\30\pm10$
P461DS46	14.2	9.5	-4.4 ± 1.5	0.86 ± 0.10	1.98 ± 0.11	0.15 ± 0.05	9.5 ± 0.5	30 ± 10

^a From DLS data.

 $^{^{}m c}$ Estimated from SAXS profile assuming $d_{
m S}=1.12\pm0.2$ nm.

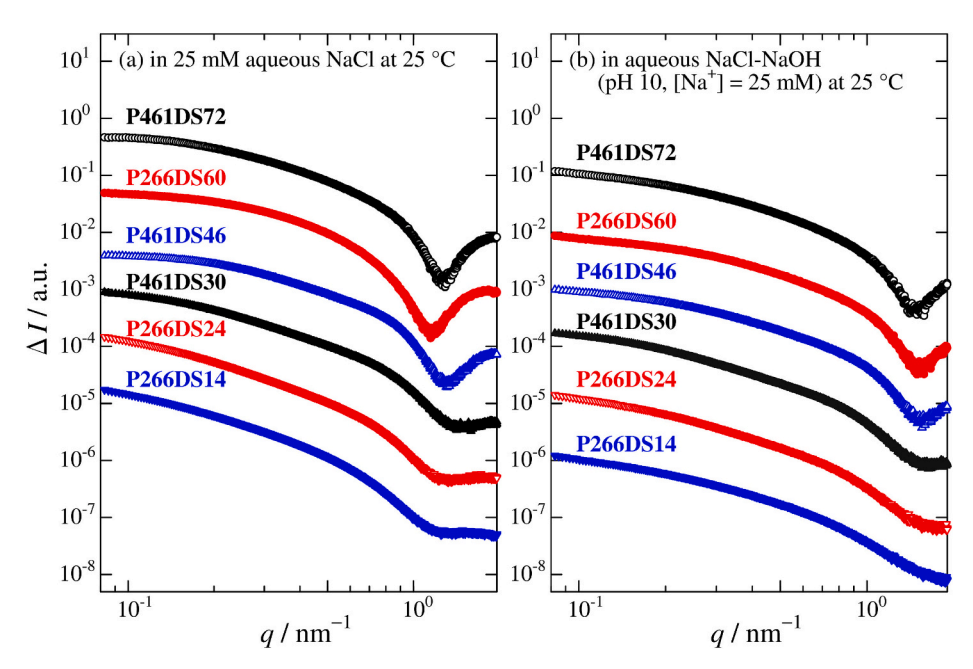


Fig. 4. Magnitude q of the scattering vector dependence of excess scattering intensity ΔI for indicated PulDS samples for with c being between 8 and 10 mg/mL in 25 mM aqueous NaCl (a) and in aqueous NaCl-NaOH (pH 10, [Na⁺] = 25 mM) (b) all at 25 °C.

Fig. S10 shows the fluorescence decay of pyrene in the presence of the indicated PulDS samples in aqueous NaCl in which natural logarithm of the ratio I(t)/I(0) is plotted against t. Since the decay curves are similar to those for random and/or alternative copolymer micelles (Kawata et al., 2007; Ueda et al., 2011) as well as PULOSA (Yang & Sato, 2020b, 2021b). As with previous works on polymeric micelles, we chose the Infelta-Tachiya kinetics (Infelta, 1979; Infelta et al., 1974; Tachiya, 1975) where excimer formation kinetics are primarily considered. The resulting expression can be written as (Yang & Sato, 2020b)

$$ln\left[\frac{I(t)}{I(0)}\right] = -\left(k_0 + \frac{k_q k_-}{k_q + k_-} \overline{n}\right) t - \left(\frac{k_q}{k_q + k_-}\right)^2 \overline{n} \left[1 - e^{-(k_q + k_-)t}\right]$$
(1)

Here, k_0 , k_E , k_- , and n^- are the fluorescence decay rate constant for an excited free pyrene, the rate constant for excimer formation in a hydrophobic part in PulDS containing two or more pyrene molecules, the rate constant for exit of a free pyrene molecule from the hydrophobic part, and the average number of pyrene molecules in a hydrophobic part, respectively. The resulting parameters from the curve fitting of the experimental data are summarized in Table S1. All data were successfully reproduced by the theoretical curves calculated by Eq. (1), although in some cases the molecular parameters cannot be unambiguously determined, as noted in Table S1. From these parameters, the number $n_{\rm hp}$ of the hydrophobic parts per PulDS molecule was calculated as follows:

$$n_{\rm hp} = \frac{[\rm Py]M_{\rm w}}{c^{\overline{n}}} \tag{2}$$

The resulting number $n_{\rm hp}$ of hydrophobic sites listed in Table 2

indicates that there should be multiple hydrophobic cores in a PulDS molecule in the solvent. The current fluorescence spectra and decay analyses strongly suggest that the PulDS molecule contains multiple micelle cores in a single PulDS chain. Another important point is that the hydrophobic part may play a crucial role in its potential applications as an emulsifier and in drug delivery systems.

3.3. Micelle structure of high DS PulDS deduced from scattering data

The SAXS-estimated radius of gyration R_g and hydrodynamic radius R_H of high DS PulDS samples are plotted against weight-average degree of polymerization $n_{\rm w}$ in Fig. 6 together with literature data for pullulan in water (or phosphate buffer) (Kato et al., 1984; Nordmeier, 1993; Watanabe & Inoko, 2011). The Rg data for PulDS are significantly smaller than those for pullulan at the same weight average degree of polymerization n_w . This is consistent with the previously investigated polymeric micelles that form flower necklaces (Uramoto et al., 2016) as illustrated in Fig. 7b. In this figure, the blue lines and red ovals in panels a and b represent the backbone and hydrophobic groups, respectively. Since the number n_{hp} of the hydrophobic core of PulDS is about 20 as shown in Table 2, it is reasonable to suppose that PulDS forms flower necklace (Ueda et al., 2011; Uramoto et al., 2016) in the solvent. It should be noted that to the best of our knowledge, this is the only theoretical model available to describe experimental scattering data for random copolymer and/or partially substituted polysaccharide derivatives. On the contrary, the $R_{\rm H}$ values are quite similar to those of pullulan especially at pH 10. This will be discussed at the end of this section, as it is closely related to the micelle structure of PulDS.

^b From Guinier plot of SAXS data.

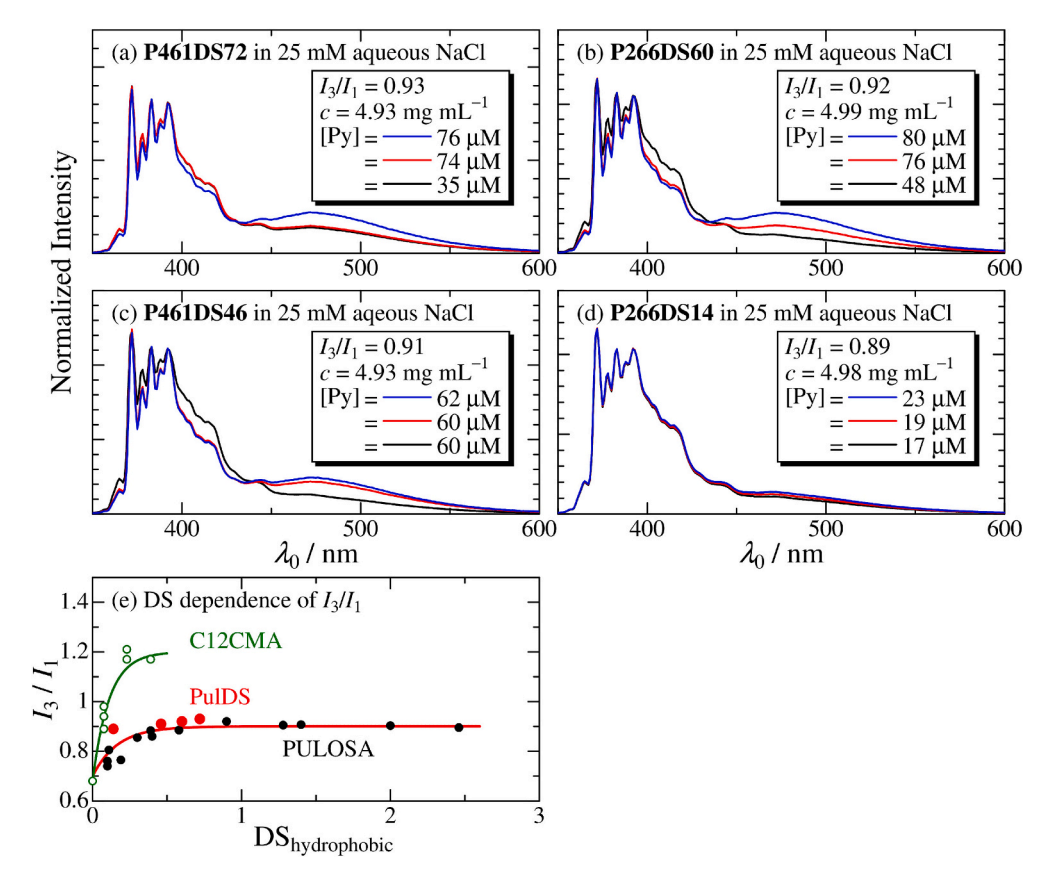


Fig. 5. Fluorescence spectra of pyrene with (a) **P461DS72**, (b) **P266DS60**, (c) **P461DS46**, (d) **P266DS14** in 25 mM aqueous NaCl at 25 °C. (e) DS dependence of I_3/I_1 for PulDS along with the literature data for PULOSA (Yang & Sato, 2020b, 2021b) and C12CMA (Kameyama et al., 2019).

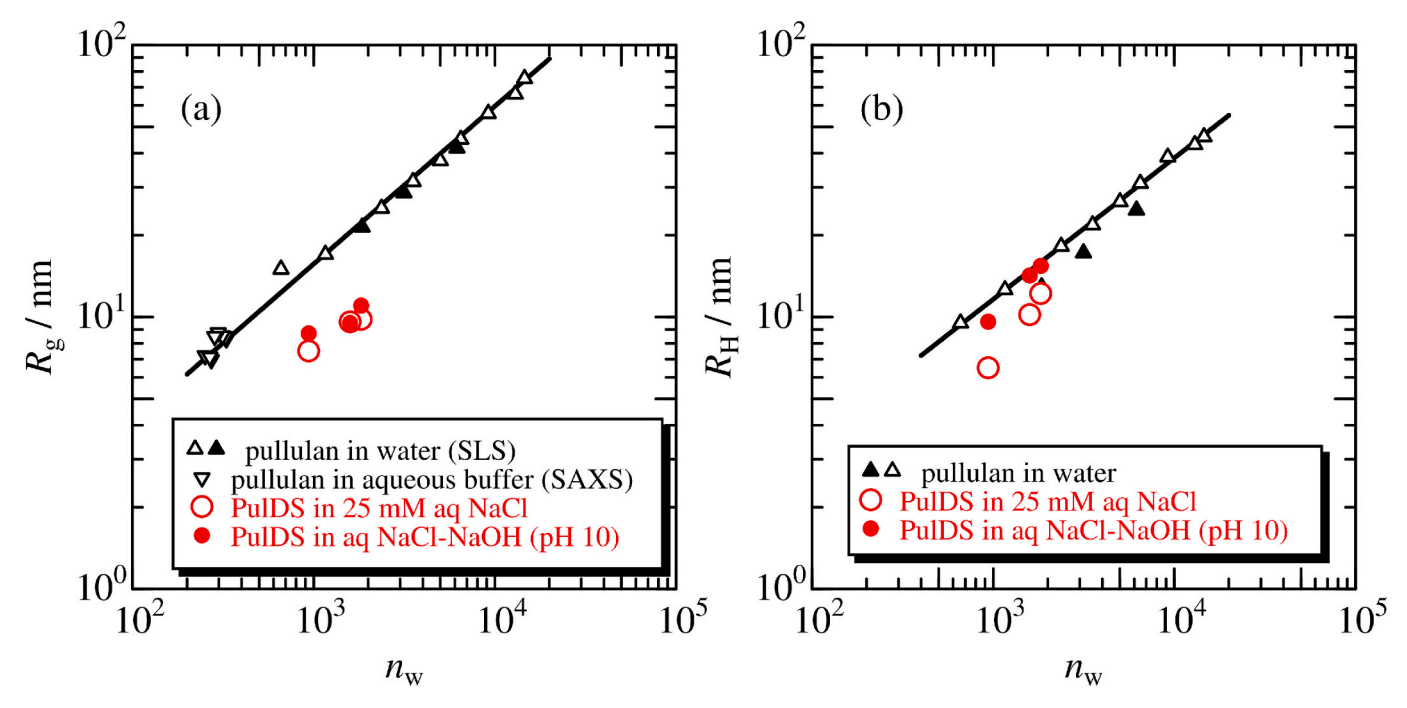
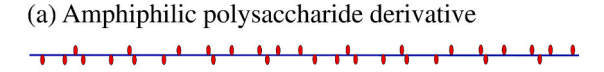
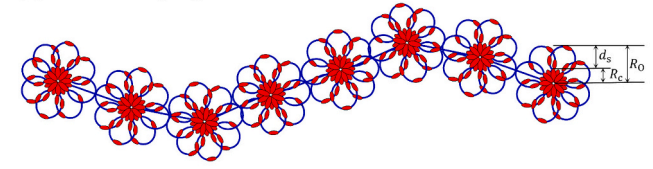


Fig. 6. Double logarithmic plots of (a) gyration radius R_g and (b) hydrodynamic radius R_H vs weight-average degree of polymerization n_w for PulDS (**P461DS72**, **P266DS60**, and **P461DS46**) along with the literature data for pullulan in water (unfilled triangles (Kato et al., 1984) and filled triangles (Nordmeier, 1993)) by SLS and that in 50 mM phosphate buffer by SAXS (invert triangles) (Watanabe & Inoko, 2011).



(b) Model of polysaccharide micelles



(c) Touched core-shell bead model

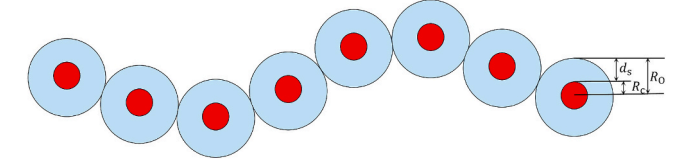


Fig. 7. Schematic illustration of the flower necklace model consisting of n_c (= 8) unit flower micelles.

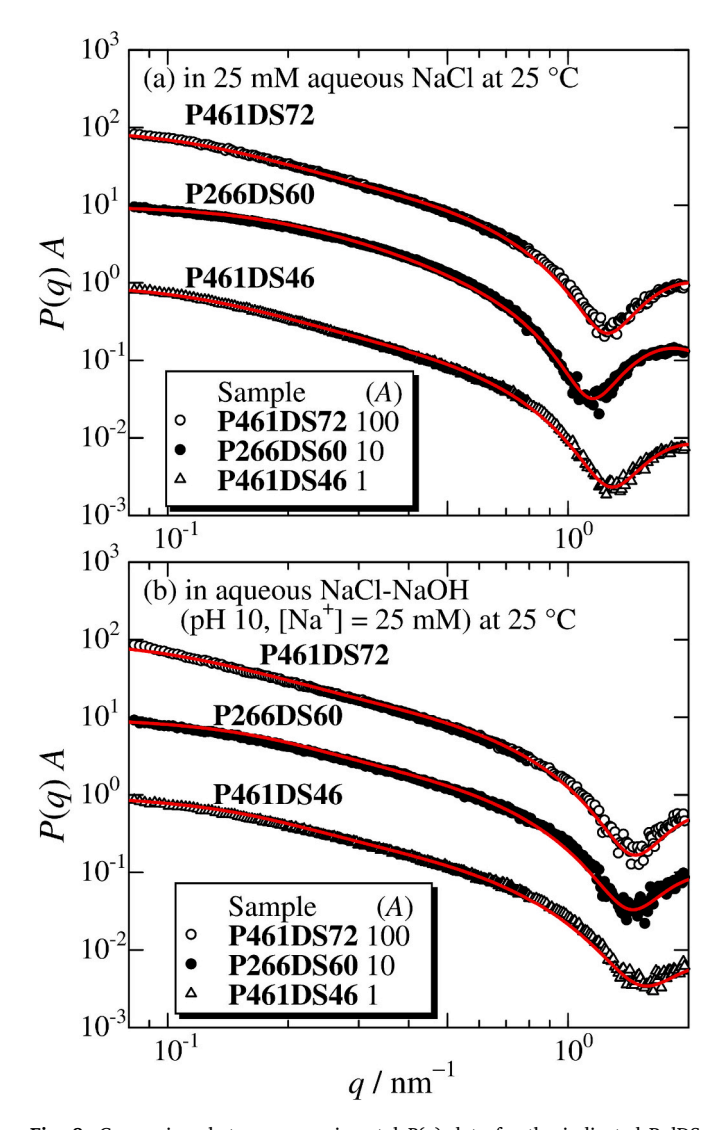


Fig. 8. Comparison between experimental P(q) data for the indicated PulDS samples with theoretical values of flower necklace model for polymer micelles in 25 mM aqueous NaCl (a) and in aqueous NaCl-NaOH (pH 10, [Na⁺] = 25 mM) (b) both at 25 °C.

Since the form factor P(q) more precisely reflects the micelle structure, we analyze here the data shown in Fig. 8. The form factor for the flower necklace $P_{\rm FN}(q)$ can be expressed as

$$P_{\text{FN}}(q) = P_{\text{KP}}(q)P_{\text{flower}}(q) \tag{3}$$

where $P_{\rm KP}(q)$ and $P_{\rm flower}(q)$ denote the form factor of the KP chain and the core-shell sphere, respectively. Here, we chose the Kratky-Porod wormlike chain (KP chain) as the backbone of the flower necklace because it can explain both the dimensional and hydrodynamic properties of most polymer chains (Yamakawa & Yoshizaki, 2016). The expression for $P_{\rm flower}(q)$ can be simplified using the touched-bead coreshell bead model as illustrated in Fig. 7(c) (Uramoto et al., 2016). It should be noted that the theory for spherical micelles (Pedersen, 1997; Pedersen & Gerstenberg, 1996) was not applied in this work because the conformation of the loop chains in the shell region may not behave as Gaussian. Of course, this coarse-graining may affect the theoretical values in the high-q region as previously pointed out for block copolymer micelles (Sanada et al., 2012). Consequently, $P_{\rm flower}(q)$ can be expressed as the form factor $P_{\rm CS}(R_{\rm C},R_{\rm O},q)$ of a core-shell sphere.

$$\begin{split} P_{\text{flower}}(q) &= P_{\text{CS}}(R_{\text{C}}, R_{\text{O}}, q) \\ &= 9 \left(\frac{\Delta \rho_{\text{r}}(sinqR_{\text{C}} - qR_{\text{C}}cosqR_{\text{C}}) + sinqR_{\text{O}} - qR_{\text{O}}cosqR_{\text{O}}}{q^3 \left(\Delta \rho_{\text{r}} R_{\text{C}}^3 + R_{\text{O}}^3 \right)} \right)^2 \end{split} \tag{4}$$

Here, $R_{\rm C}$, $R_{\rm O}$, and $\Delta \rho_{\rm r}$ are the core radius, the outer radius, and the electron density parameter, which is expressed with the excess electron densities of the core ($\Delta \rho_{\rm c}$) and the shell ($\Delta \rho_{\rm s}$) as

$$\Delta \rho_{\rm r} = \frac{\Delta \rho_{\rm C} - \Delta \rho_{\rm S}}{\Delta \rho_{\rm S}} \tag{5}$$

While the core part is mainly composed of decyl groups of PulDS, the characteristic loop chains consisting of PulDS form the shell part as shown in Fig. 7. Kawata et al. (2007) proposed that the thickness $d_{\rm S}$ ($\equiv R_{\rm O} - R_{\rm C}$) of the shell part can be estimated from the minimum size loops of the wormlike main chain, which can be calculated as $d_{\rm S} = 0.31 L_{\rm K}$ (the Kuhn segment length) from the ring closure probability of the KP chain (Yamakawa & Yoshizaki, 2016). This relationship successfully explained the size (Kawata et al., 2007; Ueda et al., 2011) as well as the SAXS data (Kameyama et al., 2019; Sato et al., 2022; Uramoto et al., 2016) of amphiphilic polymer micelles. On the other hand, the former $P_{\rm KP}(q)$ can be calculated from the known expression (Nakamura & Norisuye, 2008; Yamakawa & Yoshizaki, 2016) with the Kuhn segment length $L_{\rm K,FN}$ of the flower necklace, which reflects the chain stiffness, and the contour length L, which is represented by the number $n_{\rm C}$ of micelles in a molecule and the diameter of the micelle $R_{\rm O}$

$$L = n_{\rm C}R_{\rm O} = n_{\rm C}(R_{\rm C} + d_{\rm S}) \tag{6}$$

Assuming that the size distribution of the core radius $R_{\rm C}$ is considered by the Gaussian distribution with the mean core radius $R_{\rm C,m}$ and the standard deviation σ , $P_{\rm flower}(q)$ can be written as

$$P_{\mathrm{flower}}(q) = \frac{1}{\sqrt{\pi}} \int_{-\infty}^{\infty} P_{\mathrm{CS}} \Big(R_{\mathrm{C,m}} + \sqrt{2} \, \sigma x, R_{\mathrm{O,m}} + \sqrt{2} \, \sigma x, q \Big) exp(-x^2) \mathrm{d}x \quad (7)$$

Eventually, the theoretical P(q) can be calculated as a function of q from Eqs. (3)–(7) using the parameters $\Delta \rho_{\rm r}$, $R_{\rm C,m}$, $d_{\rm S}$, σ , $L_{\rm K, FN}$, and $n_{\rm C}$.

A curve fitting procedure was used to fit the experimental P(q) data in Fig. 8 to the theoretical values for the flower necklace. Since not all parameters can be unambiguously determined, we assume the size of the loop chain, i.e., $d_S=1.12$ nm, which is calculated from the L_K of 3.6 nm for pullulan determined from the intrinsic viscosity data (Yang & Sato, 2020a). It should be noted that we did not take the value of $\Delta \rho_r$ from the calculated method, as previously reported (Yang & Sato, 2020b), because the preferential adsorption effects on $\Delta \rho_r$ are difficult to estimate, although we would measure the dialyzed solution. The remaining five parameters of $\Delta \rho_r$, $R_{C.m.}$, σ , $L_{K.}$ FN, and n_C were determined from the

curve fitting of the P(q) data. The resulting theoretical values in Fig. 8 quantitatively reproduce the experimental data. It is noted that the R_g values for PulDS are consistent with those calculated for the flower necklace model with the parameters in Tables 2 and 3. The agreement between experimental and theoretical values is achieved in the range of $q < 3 \text{ nm}^{-1}$, as shown for two samples in Fig. S11. This is reasonable because the smooth density model cannot explain the experimental data of even the single polysaccharide derivative chain (Terao, 2009) and a collagen peptide (Terao et al., 2008) in the range of q > 3 nm⁻¹. To account for the uncertainty in the assumption of d_S , we also attempted to fit the data for the range of $d_{\rm S}=1.12$ nm \pm 0.2 nm. The resulting parameters are shown in Tables 2 and 3 with the error range of the parameters. Since the $R_{C,m}$ tends to increase with decreasing d_S , the error range of R_{O,m} values tends to be narrower as shown in the tables. Although a rather large uncertainty is found for $\Delta \rho_r$, the evaluated value does not contradict the calculated values (~ -2) for flower micelles with some assumptions as shown in the previous work (Yang & Sato, 2020b). Despite this uncertainty, the error range of $R_{C,m}$ and $R_{O,m}$ is not significant, i.e., at most ± 20 % and ± 6 %, respectively. The narrowly dispersed micelle structure can also be confirmed from the σ value, which is significantly smaller than that of pullulan octenyl (Yang & Sato, 2020b), nonenyl (Yang et al., 2024), and decenyl (Li et al., 2025) succinic acids prepared in aqueous media, clearly indicating that the flower necklace is a good model for PulDS in aqueous media. Two possible reasons can be suggested. The first is the chemical stability of the saturated side groups. The second is that we used an organic solvent system, whereas the previous study used water as the synthesis solvent, which resulted in a heterogeneous reaction as pointed out by the authors (Sato et al., 2022). Since random substitution was suggested for certain carbamate derivatives of polysaccharides prepared in the same organic solvent system, based on the spectroscopic analysis of their complexes with small molecules (Kobayashi & Terao, 2024), it is reasonable to assume that the side groups of PulDS were randomly introduced. However, it remains difficult to estimate the substituent distribution for the current PulDS samples.

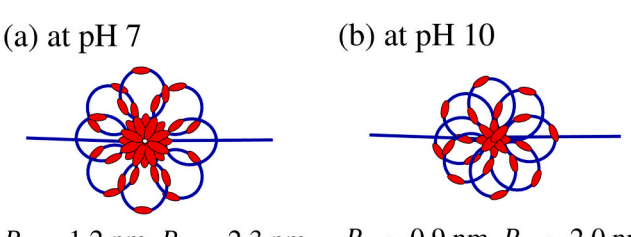
It is, however, noticed that the current n_{hp} is about 2–3 times larger than n_c , although n_{hp} is considered as the number of hydrophobic core n_c for the synthetic polymer micelles (Ueda et al., 2011). One of the possible reasons is that not only the micelle cores, as confirmed from the analyses of SAXS scattering profiles, but also some decyl groups located on the loop chains behave as a hydrophobic environment. Indeed, we have recently shown that the excimer peak of pyrene is observed for branched polysaccharide derivatives that do not form a hydrophobic core (Kobayashi & Terao, 2024). Another reason is that the estimation of $n_{\rm c}$ using the flower necklace model may have some error. If we assume that $n_c = 22$ and $L_{K.FN} = 8$ nm for **P461DS72**, the calculated theoretical values (the blue dashed curve) are compared with the experimental data in Fig. S12. The resulting R_g is the same as that for the original parameters can be calculated with the other parameters being the same as those in Table 2. When the vertically shifted theoretical values, shown as the green dotted curve, fit the experimental data well in the high q region, it indicates that the structure estimation of the unit flower micelle is still correct. This discrepancy in n_c might be due to the fact that the statistics of the flower necklace do not follow the wormlike chain. In fact, when the RH was calculated for the wormlike cylinder model (Yamakawa & Fujii, 1973; Yamakawa & Yoshizaki, 2016), using the Kuhn segment length $L_{K,FN}$ in Table 2, the contour length was calculated as $2n_cR_{O,m}$, and the diameter d was assumed to be the same as $2R_{O,m}$, the calculated $R_{\rm H}$ for P461DS72 was appreciably smaller (7.7 nm) than the experimental value. A similar discrepancy was found for the other all samples. On the contrary, if we choose $n_c = 22$, the resulting R_H is calculated to be 11.9 nm, which is quite close to the experimental value. It should be noted that the similar RH values for PulDS and pullulan (Fig. 7b) with the same degree of polymerization are incidental, despite their considerably different conformations. We leave further discussion because there are many arguments for the conformation even for simple

polyelectrolytes in aqueous media, especially at low ionic strength (Yamakawa & Yoshizaki, 2016).

Another important point is that both R_{C,m} and R_{O,m} are appreciably smaller at pH 10 than at pH 7. Considering that A_2 is twice as large at pH 10, some OH groups on the glycosidic ring are ionized at pH 10 and the resulting electrostatic repulsion reduces the size of the micelle core and makes the intermolecular interactions more repulsive. This is probably reasonable because the pK_a of a neutral saccharide molecule is around 12, e.g., the pKa of cyclodextrin (Szejtli, 1998). Assuming that the hydrophobic core is composed of decyl group and the density is the same as that of decan at room temperature, the number of hydrophobic groups $n_{\rm h}$ in the micelle cores of a PulDS molecule can be calculated. Therefore, the ratio n_h / n_d of n_h to the number n_d of decyl groups in a PulDS molecule is calculated to be 0.15 \pm 0.04, 0.35 \pm 0.08, and 0.27 \pm 0.04 for P461DS72, P266DS60, and P461DS46, respectively, at pH 7. Similar estimates were also made at pH 10 as $n_h / n_d = 0.11 \pm 0.03, 0.17$ \pm 0.05, and 0.11 \pm 0.03 for P461DS72, P266DS60, and P461DS46, respectively. These results indicate that only a certain amount of hydrophobic decyl groups are located in the micelle core, and a larger amount of them are located on the loop chains, as in the case of previous works (Sato et al., 2022; Uramoto et al., 2016). The value of n_h / n_d at pH 10 tends to be smaller than that at pH 7. In other words, there are more decyl groups outside the hydrophobic core at pH = 10. This is most likely due to the enhanced repulsion caused by slightly ionized hydroxyl groups, as described above. These features are summarized in Fig. 9. It is also noted that despite the number of hydrophobic sites on the loop chain, a relatively high A2 was observed. This is most likely because not only electrostatic repulsion, but also topological interactions often observed for ring polymers (Terao et al., 2013) increase the A_2 value in solution.

4. Conclusions

A pullulan-based amphiphilic copolymer, decyl succinic anhydridemodified pullulan (PulDS), was prepared to investigate its solubility in aqueous media and the resulting micelle structure. PulDS samples with a degree of substitution DS between 0.46 and 0.72 were found to be molecularly dispersed in aqueous NaCl, whereas previously investigated pullulan-based amphiphilic polymers (Li et al., 2025; Yang et al., 2024; Yang & Sato, 2020b) tend to form large aggregates. Furthermore, SAXS measurements revealed a narrowly dispersed micelle structure for the PulDS samples. The evaluated size dispersity parameter (σ) is, to the best of our knowledge, the smallest among the succinic anhydride derivatives of polysaccharides studied to date. The fluorescence, dimensional, and hydrodynamic properties of these micelles were explained by the flower necklace model, suggesting that the amphiphilic polysaccharide derivative synthesized as demonstrated in this study could serve as a good model for polysaccharide-based micelles. Another finding was that the micelle size at high pH (pH = 10) was appreciably smaller than that at neutral pH, likely due to increased repulsive intramolecular interactions resulting from the partial ionization of hydroxyl



 $R_{\rm C} \sim 1.2 \text{ nm}, R_{\rm O} \sim 2.3 \text{ nm}$ $R_{\rm C} \sim 0.9 \text{ nm}, R_{\rm O} \sim 2.0 \text{ nm}$ $A_2 \sim 1 \times 10^{-4} \text{mol m}^3 \text{kg}^{-2}$ $A_2 \sim 2 \times 10^{-4} \text{mol m}^3 \text{kg}^{-2}$ $\sigma \sim 0.15$

Fig. 9. Schematic illustration of the flower micelles of PulDS in 25 mM aqueous NaCl (a) and in aqueous NaCl-NaOH (pH 10, $[Na^+] = 25 \text{ mM}$) (b) both at 25 °C.

groups on the polysaccharide backbone. In conclusion, the high solubility, well-defined micellar structure, and pH-responsive behavior of PulDS make it an excellent candidate for developing innovative solutions in healthcare and food-related applications, especially when a more cost-effective synthetic method is established. Furthermore, the synthesis procedure demonstrated in this study could be extended to a broad range of polysaccharides and succinic anhydride derivatives, enabling the preparation of various types of amphiphilic polysaccharide derivatives.

CRediT authorship contribution statement

Risa Suenaga: Writing – original draft, Investigation, Formal analysis, Data curation. **Yuzu Komuro:** Validation, Writing – review & editing. **Ken Terao:** Writing – review & editing, Writing – original draft, Supervision, Project administration, Funding acquisition, Formal analysis, Conceptualization.

Declaration of competing interest

The authors declare the following financial interests/personal relationships which may be considered as potential competing interests:

Ken Terao reports financial support was provided by Japan Society for the Promotion of Science. If there are other authors, they declare that they have no known competing financial interests or personal relationships that could have appeared to influence the work reported in this paper.

Acknowledgments

The authors are grateful to Dr. Noboru Ohta (SPring-8) for the SAXS measurements. The synchrotron radiation experiments were performed at the BL40B2 in SPring-8 with the approval of the Japan Synchrotron Radiation Research Institute (JASRI) (proposal Nos. 2022B1120, 2023A1111, 2023A1112, 2023B1124, and 2023B1125). This work was the result of the use of research equipment (NMR) shared under the MEXT Project for promoting public utilization of advanced research infrastructure (Program for supporting construction of core facilities) Grant No. JPMXS0441200023. This work was partially supported by Japan Society for the Promotion of Science (JSPS) KAKENHI grant Nos. JP20H02788, JP23H02011, and JP23K26704.

Appendix A. Supplementary data

Additional figures for ¹H NMR, SEC-MALS, SLS, DLS, SAXS, fluorescence decay, and a table for micelle parameters. Supplementary data to this article can be found online at https://doi.org/10.1016/j.carbpol. 2025.123504.

Data availability

Data will be made available on request.

References

- Akiyoshi, K., Deguchi, S., Moriguchi, N., Yamaguchi, S., & Sunamoto, J. (1993). Self-aggregates of hydrophobized polysaccharides in water formation and characteristics of nanoparticles. *Macromolecules*, 26, 3062–3068. https://doi.org/10.1021/Ma00064a011
- Aquinas, N., Chithra, C. H., & Bhat, M. R. (2024). Progress in bioproduction, characterization and applications of pullulan: A review. *Polymer Bulletin*, 81, 12347–12382. https://doi.org/10.1007/s00289-024-05300-2
- Bruneel, D., Schacht, E., & Debruyn, A. (1993). Structural-analysis of succinoylated and chloroformate activated pullulan - Nmr-study in Dmso solution. *Journal of Carbohydrate Chemistry*, 12, 769–778. https://doi.org/10.1080/ 07328309308019006
- Cao, J., Wu, J., Yang, P., Qian, K., Cheng, Y., Xu, M., ... Zhang, Q. (2023). Dual enzyme cascade-activated popcorn-like nanoparticles efficiently remodeled stellate cells to

- alleviate pancreatic desmoplasia. ACS Nano, 17, 19793–19809. https://doi.org/
- Cruz-Santos, M. M., Antunes, F. A. F., Arruda, G. L., Shibukawa, V. P., Prado, C. A., Ortiz-Silos, N., ... Santos, J. C. (2023). Production and applications of pullulan from lignocellulosic biomass: Challenges and perspectives. *Bioresource Technology*, 385, Article 129460. https://doi.org/10.1016/j.biortech.2023.129460
- de Souza, C. K., Ghosh, T., Lukhmana, N., Tahiliani, S., Priyadarshi, R., Hoffmann, T. G., ... Han, S. S. (2023). Pullulan as a sustainable biopolymer for versatile applications: A review. *Materials Today Communications*, 36, Article 106477. https://doi.org/ 10.1016/j.mtcomm.2023.106477
- Eenschooten, C., Vaccaro, A., Delie, F., Guillaumie, F., Tommeraas, K., Kontogeorgis, G. M., ... Gurny, R. (2012). Novel self-associative and multiphasic nanostructured soft carriers based on amphiphilic hyaluronic acid derivatives. *Carbohydrate Polymers*, 87, 444–451. https://doi.org/10.1016/j. carbool.2011.08.004
- Ganie, S. A., Rather, L. J., Assiri, M. A., & Li, Q. (2024). Recent innovations (2020–2023) in the approaches for the chemical functionalization of curdlan and pullulan: A minireview. *International Journal of Biological Macromolecules*, 260, Article 129412. https://doi.org/10.1016/j.ijbiomac.2024.129412
- Glatter, O., & Kratky, O. (1982). Small angle X-ray scattering. London: Academic Press.
- Goddard, E. D., Turro, N. J., Kuo, P. L., & Ananthapadmanabhan, K. P. (1985). Fluorescence probes for critical micelle concentration determination. *Langmuir*, 1, 352–355. https://doi.org/10.1021/la00063a015
- Hongbo, T., Manxin, W., Yanping, L., & Xiaojun, L. (2022). Octenyl succinate hydroxypropyl acidolysis tamarind gum: Synthesis, optimization, structure and properties. *Polymer Journal*, 55, 13–25. https://doi.org/10.1038/s41428-022-00702-
- Ikkene, D., Arteni, A. A., Ouldali, M., Six, J. L., & Ferji, K. (2020). Self-assembly of amphiphilic copolymers containing polysaccharide: PISA nanoprecipitation, and the temperature effect. *Polymer Chemistry*, 11, 4729–4740. https://doi.org/10.1039/ d0py00407c
- Infelta, P. P. (1979). Fluorescence quenching in micellar solutions and its application to the determination of aggregation numbers. *Chemical Physics Letters*, 61, 88–91. https://doi.org/10.1016/0009-2614(79)85092-7
- Infelta, P. P., Gratzel, M., & Thomas, J. K. (1974). Luminescence decay of hydrophobic molecules solubilized in aqueous micellar systems - kinetic-model. *Journal of Physical Chemistry*, 78, 190–195. https://doi.org/10.1021/j100595a021
- Inomoto, N., Osaka, N., Suzuki, T., Hasegawa, U., Ozawa, Y., Endo, H., Akiyoshi, K., & Shibayama, M. (2009). Interaction of nanogel with cyclodextrin or protein: Study by dynamic light scattering and small-angle neutron scattering. *Polymer*, 50, 541–546. https://doi.org/10.1016/j.polymer.2008.11.001
- Kalyanasundaram, K., & Thomas, J. K. (1977). Environmental effects on vibronic band intensities in pyrene monomer fluorescence and their application in studies of micellar systems. *Journal of the American Chemical Society*, 99, 2039–2044. https:// doi.org/10.1021/Ja00449a004
- Kameyama, Y., Kitamura, S., Sato, T., & Terao, K. (2019). Self-assembly of amphiphilic amylose derivatives in aqueous media. *Langmuir*, 35, 6719–6726. https://doi.org/ 10.1021/acs.langmuir.9b00985
- Kato, T., Katsuki, T., & Takahashi, A. (1984). Static and dynamic properties of pullulan in a dilute-solution. *Macromolecules*, 17, 1726–1730. https://doi.org/10.1021/ ma00139a016
- Kawata, T., Hashidzume, A., & Sato, T. (2007). Micellar structure of amphiphilic statistical copolymers bearing dodecyl hydrophobes in aqueous media. *Macromolecules*, 40, 1174–1180. https://doi.org/10.1021/ma062299x
- Kimura, S., Kochi, R., Kitamura, S., & Terao, K. (2020). A temperature responsive polysaccharide derivative in aqueous solution: Amylose ethyl carbamates. ACS Applied Polymer Materials, 2, 2426–2433. https://doi.org/10.1021/acsapm.0c00366
- Kishimoto, A., Mizuguchi, M., Ryoki, A., & Terao, K. (2022). Molecular structure and chiral recognition ability of highly branched cyclic dextrin carbamate derivative. *Carbohydrate Polymers*, 290, Article 119491. https://doi.org/10.1016/j. carbpol.2022.119491
- Kobayashi, A., & Terao, K. (2024). Highly branched thermoresponsive polysaccharide derivative in water. Partly substituted highly branched cyclic dextrin ethylcarbamate. Carbohydrate Polymers, 343, Article 122473. https://doi.org/ 10.1016/j.carbpol.2024.122473
- Kono, H., Hibino, M., Ida, D., Ouchi, M., & Terashima, T. (2023). Self-assembly of amphiphilic alternating copolymers by chain folding in water: From uniform composition and sequence to monodisperse micelles. *Macromolecules*, 56, 6086–6098. https://doi.org/10.1021/acs.macromol.3c00649
- Kubota, T., Yamamoto, C., & Okamoto, Y. (2000). Tris(cyclohexylcarbamate)s of cellulose and amylose as potential chiral stationary phases for high-performance liquid chromatography and thin-layer chromatography. *Journal of the American Chemical Society*, 122, 4056–4059. https://doi.org/10.1021/Ja992421q
- Li, W. Z., Liu, Y. T., Sheng, Y. G., & Yang, J. (2025). Micellar structure of decenyl succinic anhydride modified pullulan with degree of substitution dependence in aqueous solution. *Carbohydrate Polymers*, 347, Article 122700. https://doi.org/10.1016/j. carbpol.2024.122700
- Liang, Q., Cheng, Z., & Qin, L. (2024). Advanced nanoparticles in osteoarthritis treatment. Biomaterials Translational, 5, 95–113. https://doi.org/10.12336/ biomatertransl.2024.02.002
- Lianos, P., & Zana, R. (1980). Use of pyrene excimer formation to study the effect of sodium chloride on the structure of sodium dodecyl sulfate micelles. *The Journal of Physical Chemistry*, 84, 3339–3341. https://doi.org/10.1021/j100462a003
- Mayol, L., Biondi, M., Russo, L., Malle, B. M., Schwach-Abdellaoui, K., & Borzacchiello, A. (2014). Amphiphilic hyaluronic acid derivatives toward the design

- of micelles for the sustained delivery of hydrophobic drugs. Carbohydrate Polymers, 102, 110-116. https://doi.org/10.1016/j.carbpol.2013.11.003
- Nakamura, Y., & Norisuye, T. (2008). Brush-like polymers. In R. Borsali, & R. Pecora (Eds.), Soft matter characterization (pp. 235–286). Netherlands: Springer. https://doi. org/10.1007/978-1-4020-4465-6_5.
- Nakata, Y., Kitamura, S., & Terao, K. (2024). Dual thermoresponsive polysaccharide derivative – Water system. Partially substituted amylose butylcarbamate in water. *Carbohydrate Polymers*, 325, Article 121587. https://doi.org/10.1016/j. carbpol.2023.121587
- Narita, T., Terao, K., Dobashi, T., Nagasawa, N., & Yoshii, F. (2004). Preparation and characterization of core-shell nanoparticles hardened by gamma-ray. *Colloids and Surfaces B: Biointerfaces*, 38, 187–190. https://doi.org/10.1016/j. colsurfb.2004.02.021
- Nishimura, T., Fujii, S., Sakurai, K., Sasaki, Y., & Akiyoshi, K. (2021). Manipulating the morphology of amphiphilic graft-copolymer assemblies by adjusting the flexibility of the main chain. *Macromolecules*, 54, 7003–7009. https://doi.org/10.1021/acs. macromol.1c01030
- Nishimura, T., Shishi, S., Sasaki, Y., & Akiyoshi, K. (2020). Thermoresponsive polysaccharide graft polymer vesicles with tunable size and structural memory. *Journal of the American Chemical Society*, 142, 11784–11790. https://doi.org/ 10.1021/j.jcsc.0623200
- Nordmeier, E. (1993). Static and dynamic light-scattering solution behavior of pullulan and dextran in comparison. *Journal of Physical Chemistry*, 97, 5770–5785. https://doi.org/10.1021/j100123a050
- Pedersen, J. S. (1997). Analysis of small-angle scattering data from colloids and polymer solutions: Modeling and least-squares fitting. Advances in Colloid and Interface Science, 70, 171–210. https://doi.org/10.1016/S0001-8686(97)00312-6
- Pedersen, J. S., & Gerstenberg, M. C. (1996). Scattering form factor of block copolymer micelles. *Macromolecules*, 29, 1363–1365. https://doi.org/10.1021/Ma9512115
- Prajapati, V. D., Jani, G. K., & Khanda, S. M. (2013). Pullulan: An exopolysaccharide and its various applications. *Carbohydrate Polymers*, 95, 540–549. https://doi.org/ 10.1016/j.carbpol.2013.02.082
- Ridella, F., Carpintero, M., Marcet, I., Matos, M., Gutierrez, G., Rendueles, M., & Diaz, M. (2024). Esterification of dextran by octenyl succinic anhydride (OSA): Physicochemical characterization and functional properties assessment. Carbohydrate Polymers, 340, Article 122300. https://doi.org/10.1016/j.carbpol.2024.122300
- Sanada, Y., Akiba, I., Hashida, S., Sakurai, K., Shiraishi, K., Yokoyama, M., Yagi, N., Shinohara, Y., & Amemiya, Y. (2012). Composition dependence of the micellar architecture made from poly(ethylene glycol)-block-poly(partially benzyl-esterified aspartic acid). *Journal of Physical Chemistry B*, 116, 8241–8250. https://doi.org/ 10.1021/jp300936d
- Sato, T., Yang, J., & Terao, K. (2022). Micellar structure of hydrophobically modified polysaccharides in aqueous solution. *Polymer Journal*, 54, 403–412. https://doi.org/ 10.1038/s41428-021-00561-4
- Shimizu, N., Yatabe, K., Nagatani, Y., Saijyo, S., Kosuge, T., & Igarashi, N. (2016). Software development for analysis of small-angle X-ray scattering data. AIP Conference Proceedings, 1741, Article 050017. https://doi.org/10.1063/1.4952937
- Six, J. L., & Ferji, K. (2019). Polymerization induced self-assembly: An opportunity toward the self-assembly of polysaccharide-containing copolymers into high-order morphologies. *Polymer Chemistry*, 10, 45–53. https://doi.org/10.1039/c8pv01295d
- Sonam Jain, P. S. S., Malvi, R., & Gupta, B. (2013). Cellulose derivatives as thermoresponsive polymer: An overview: ssue. 12. https://doi.org/10.7324/ JAPS.2013.31225
- Sweedman, M. C., Tizzotti, M. J., Schafer, C., & Gilbert, R. G. (2013). Structure and physicochemical properties of octenyl succinic anhydride modified starches: A review. Carbohydrate Polymers, 92, 905–920. https://doi.org/10.1016/j. carbpol.2012.09.040
- Szejtli, J. (1998). Introduction and general overview of cyclodextrin chemistry. Chemical Reviews, 98, 1743–1754. https://doi.org/10.1021/cr970022c
- Tachiya, M. (1975). Application of a generating function to reaction-kinetics in micelles-kinetics of quenching of luminescent probes in micelles. *Chemical Physics Letters*, 33, 289–292. https://doi.org/10.1016/0009-2614(75)80158-8
- Terao, K. (2009). Dimensional and hydrodynamic properties of amylose tris (phenylcarbamate) in various solvents. *Journal of Physics: Conference Series*, 184, Article 012006. https://doi.org/10.1088/1742-6596/184/1/012006

- Terao, K., Mizuno, K., Murashima, M., Kita, Y., Hongo, C., Okuyama, K., ... Bächinger, H. P. (2008). Chain dimensions and hydration behavior of collagen model peptides in aqueous solution: [glycyl-4(R)-hydroxyprolyl-4(R)-hydroxyproline]n, [glycylprolyl-4(R)-hydroxyproline]n, and some related model peptides. Macromolecules, 41, 7203–7210. https://doi.org/10.1021/ma800790w
- Terao, K., Shigeuchi, K., Oyamada, K., Kitamura, S., & Sato, T. (2013). Solution properties of a cyclic chain having tunable chain stiffness: Cyclic amylose Tris(*n*-butylcarbamate) in Θ and good solvents. *Macromolecules*, 46, 5355–5362. https://doi.org/10.1021/ma400774r
- Thakur, A., Sharma, S., Naman, S., & Baldi, A. (2023). Pullulan based polymeric novel drug delivery systems: A review on current state of art and prospects. *Journal of Drug Delivery Science and Technology*, 90, Article 105117. https://doi.org/10.1016/j. iddst 2023 105117
- Tizzotti, M. J., Sweedman, M. C., Tang, D., Schaefer, C., & Gilbert, R. G. (2011). New (1)h NMR procedure for the characterization of native and modified food-grade starches. Journal of Agricultural and Food Chemistry, 59, 6913–6919. https://doi.org/10.1021/ipp.12009.
- Ueda, M., Hashidzume, A., & Sato, T. (2011). Unicore—multicore transition of the micelle formed by an amphiphilic alternating copolymer in aqueous media by changing molecular weight. *Macromolecules*, 44, 2970–2977. https://doi.org/10.1021/ pp.100635v
- Uramoto, K., Takahashi, R., Terao, K., & Sato, T. (2016). Local and global conformations of flower micelles and flower necklaces formed by an amphiphilic alternating copolymer in aqueous solution. *Polymer Journal*, 48, 863–867. https://doi.org/
- Watanabe, Y., & Inoko, Y. (2011). Further application of size-exclusion chromatography combined with small-angle X-ray scattering optics for characterization of biological macromolecules. *Analytical and Bioanalytical Chemistry*, 399, 1449–1453. https:// doi.org/10.1007/s00216-010-4140-7
- Wu, Z., Li, H., Zhao, X., Ye, F., & Zhao, G. (2022). Hydrophobically modified polysaccharides and their self-assembled systems: A review on structures and food applications. *Carbohydrate Polymers*, 284, Article 119182. https://doi.org/10.1016/ j.carbpol.2022.119182
- Wu, Z., Zhao, C., Huang, Y., Ye, F., & Zhao, G. (2020). Molecular mechanism underlying the effects of temperature and pH on the size and surface charge of octenylsuccinated oat beta-glucan aggregates. *Carbohydrate Polymers*, 237, Article 116115. https://doi.org/10.1016/j.carbpol.2020.116115
- Wu, Z., Zhao, C. Y., Li, R. H., Ye, F. Y., Zhou, Y., & Zhao, G. H. (2019). Insights into micellization of octenylsuccinated oat β-glucan and uptake and controlled release of β-carotene by the resultant micelles. *Journal of Agricultural and Food Chemistry*, 67, 7416–7427. https://doi.org/10.1021/acs.jafc.8b06645
- Yamakawa, H., & Fujii, M. (1973). Translational friction coefficient of wormlike chains. Macromolecules, 6, 407–415. https://doi.org/10.1021/Ma60033a018
- Yamakawa, H., & Yoshizaki, T. (2016). Helical wormlike chains in polymer solutions (2nd ed.). Berlin, Germany: Springer. https://doi.org/10.1007/978-3-662-48716-7
- Yang, J., Chen, H. W., Li, W. Z., & Yan, F. (2024). Micellar structure of nonenyl succinic anhydride modified pullulan in aqueous solution. *Polymer*, 296, Article 126766. https://doi.org/10.1016/j.polymer.2024.126766
- Yang, J., & Sato, T. (2020a). Conformation of pullulan in aqueous solution studied by small-angle X-ray scattering. *Polymers (Basel)*, 12, 1266. https://doi.org/10.3390/ polym12061266
- Yang, J., & Sato, T. (2020b). Micellar structure of a hydrophobically modified pullulan in an aqueous solution. *Macromolecules*, 53, 7970–7979. https://doi.org/10.1021/acs. macromol.0c01319
- Yang, J., & Sato, T. (2021a). Characterization of the micelle formed by a Hydrophobically modified pullulan in aqueous solution: Size exclusion chromatography. *Polymers*, 13, 1237. https://doi.org/10.3390/polym13081237
- Yang, J., & Sato, T. (2021b). Transition from the random coil to the flower necklace of a hydrophobically modified pullulan in aqueous solution by changing the degree of substitution. *Polymer*, 214, Article 123346. https://doi.org/10.1016/j. polymer.2020.123346
- Zhou, D., Wei, Y., Sheng, S., Wang, M., Lv, J., Zhao, B., ... Su, J. (2024). MMP13-targeted siRNA-loaded micelles for diagnosis and treatment of posttraumatic osteoarthritis. *Bioactive Materials*, 37, 378–392. https://doi.org/10.1016/j.bioactmat.2024.04.010